A constitutive equation for thixotropic suspensions with yield stress by coarse-graining a population balance model: Supplemental Material

Paul M. Mwasame, R. B. Diemer, Antony N. Beris, Norman J. Wagner[1]

Center for Molecular and Engineering Thermodynamics, Department of Chemical and Biomolecular Engineering, University of Delaware, Newark, DE 19716

1. Model Fits to Step-up Experiments

The model fits to step-up experimental, used in fitting the model parameters, are presented in Fig. **??**.

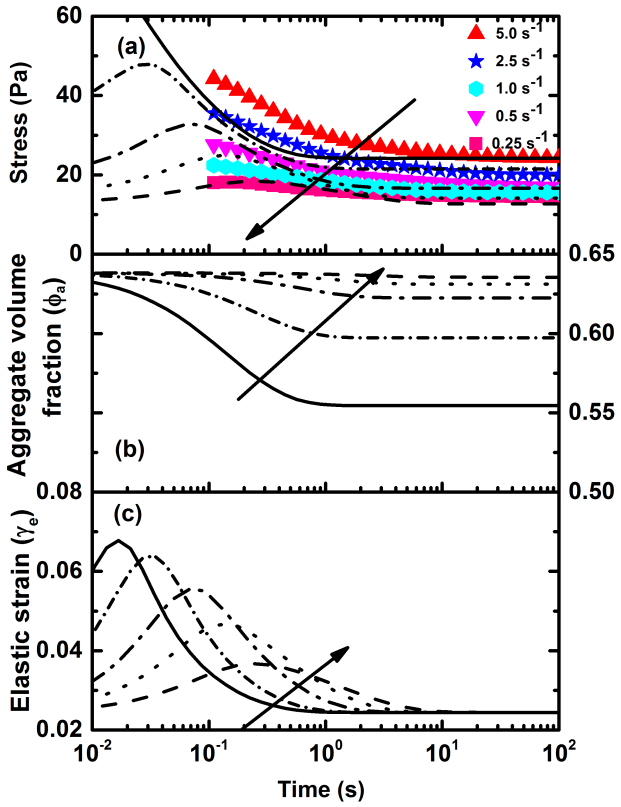

Figure S1: Comparison of model fits for a step-up experiment. The initial shear rate is 0.1 s^{-1} and the final shear rate is indicated on the plot. Model predictions correspond to shear rate of 0.25 s^{-1} to 5 s^{-1} from bottom to top. Arrows indicate lowest to highest final shear rate. (a) Model fits showing stress as a function of time. (b) Microstructural prediction of the aggregate volume fraction corresponding to the fits to rheological data. (c)The elastic strain as a function of time corresponding to the fits to the rheological data.

2. LAOS Elastic Lissajous Plot

The elastic Lissajous projections of the model predictions of the LAOS shear stress as a function of the applied strain over a single period of alternance are presented. The elastic Lissajous projections in Fig. **??** below are complementary and equivalent to the viscous Lissajous projections presented in Fig. 7 in the main paper corresponding to a frequency of 0.1 s^{-1} and a strain amplitude of 10.

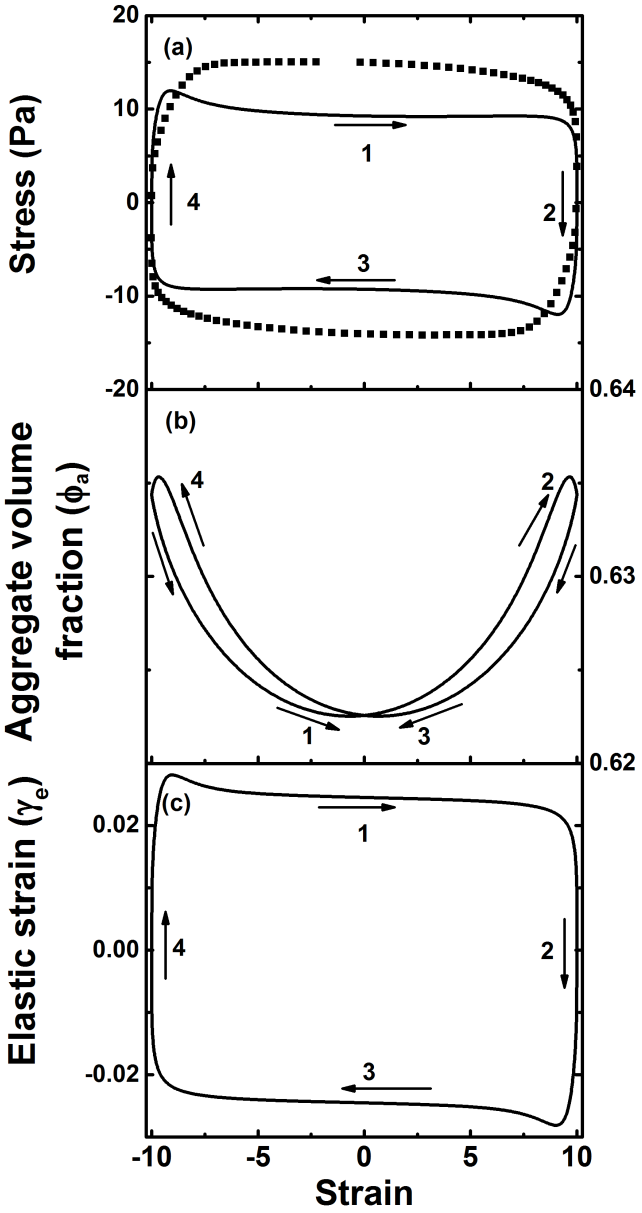

Figure S2: The elastic Lissajous projections of a LAOS experiment showing (a) the predictions of the shear stress as a function of strain, (b) the aggregate volume fraction as a function of strain and (c) the elastic strain in the material as a function of strain. ω=0.1 s^{-1} and γ_o=10 are the imposed strain amplitude and oscillatory frequency respectively

3. UD-LAOS Elastic Lissajous Plot

The elastic Lissajous projections of the model predictions of the UD-LAOS shear stress as a function of the applied strain over a single period of alternance are presented. The elastic Lissajous projections in Fig. **??** below are complementary and equivalent to the viscous Lissajous projections presented in Fig. 8 in the main paper corresponding to a frequency of 1 s^{-1} and a strain amplitude of 10.

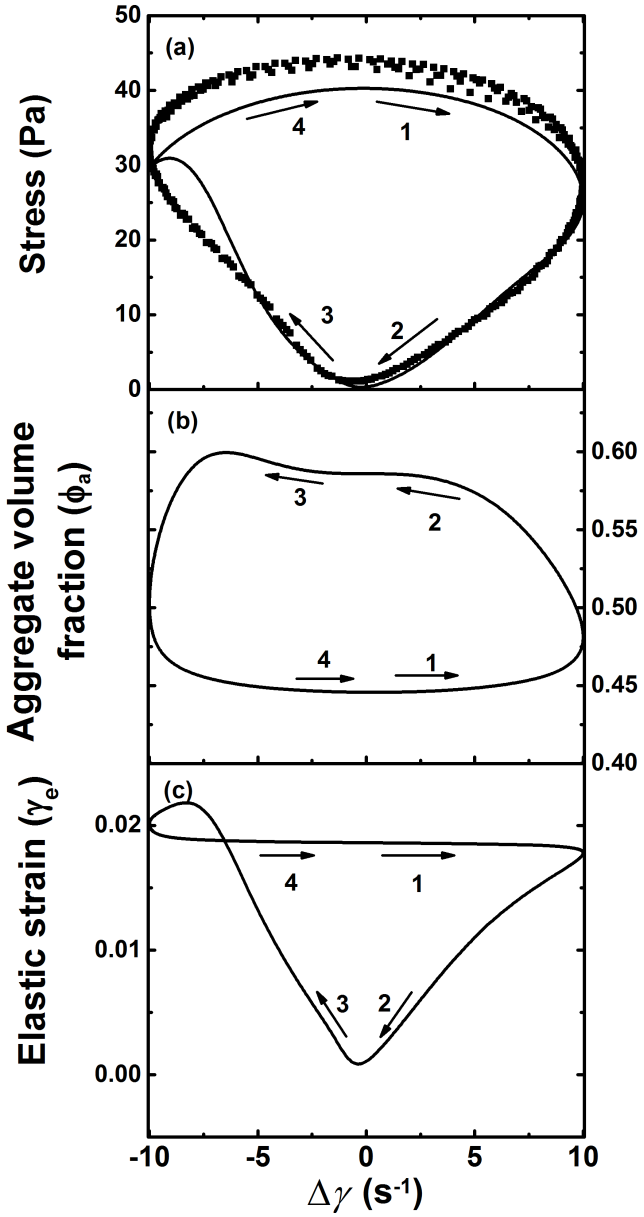

Figure S3: The elastic Lissajous projections of a UD-LAOS experiment. The shear strain is defined as $\Delta\gamma = \gamma_o sin(\omega t) - \gamma_o t$ showing (a) the predictions of the shear stress as a function of strain, (b) the aggregate volume fraction as a function of strain and (c) the elastic strain in the material as a function of strain. ω=10 and γ_o=1 s^{-1} are the imposed strain amplitude and oscillatory frequency respectively

4. Full set of Elastic and Viscous LAOS Lissajous Plots

A set of viscous Lissajous projections showing LAOS shear stress as a function of shear rate for a single period of steady alternance at various frequencies and strain amplitudes is presented in Figs. **??** and **??** below.

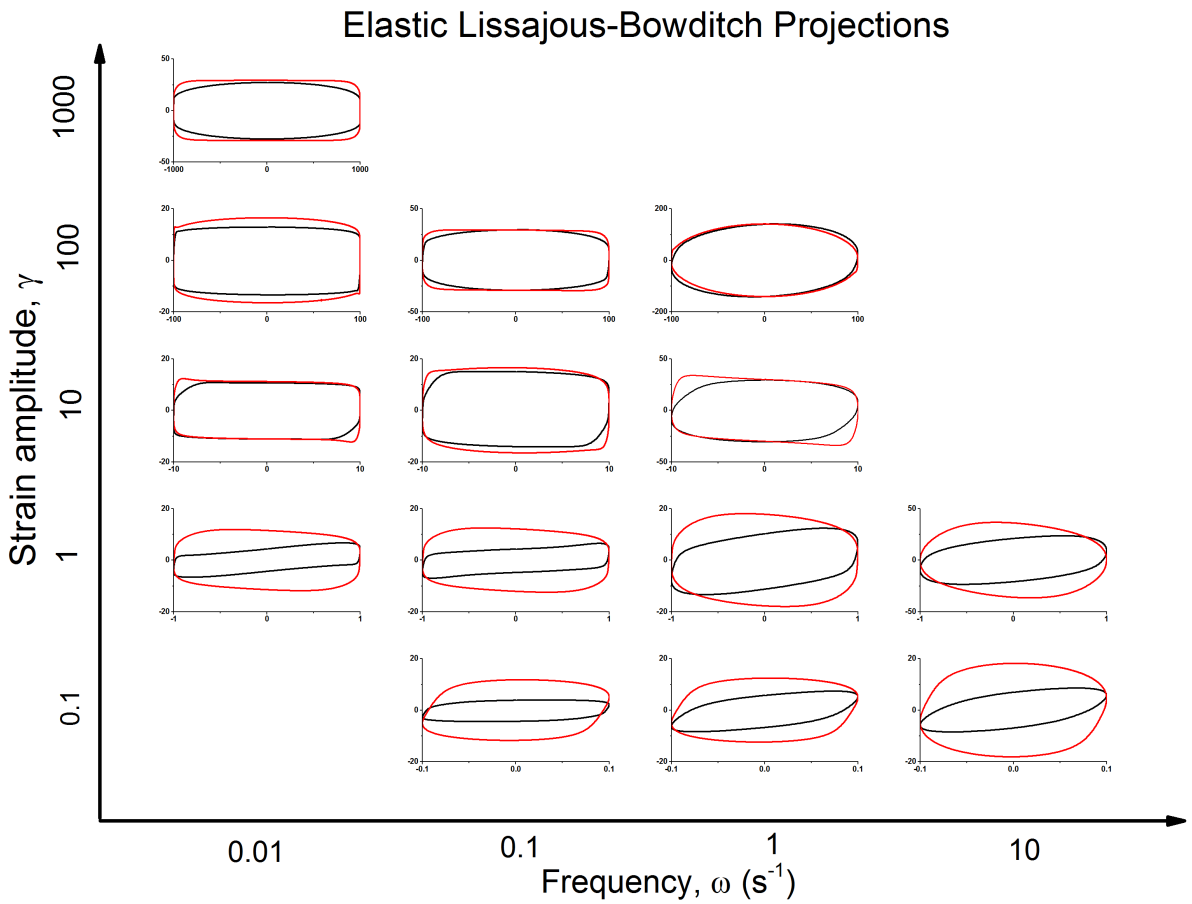

Figure S4: Elastic Lissajous model predictions of LAOS experiments at different strain amplitudes (γ) and frequencies (ω). The x-axis on the inset figures is the strain rate (s^{-1}) and the y-axis is the shear stress (Pa).

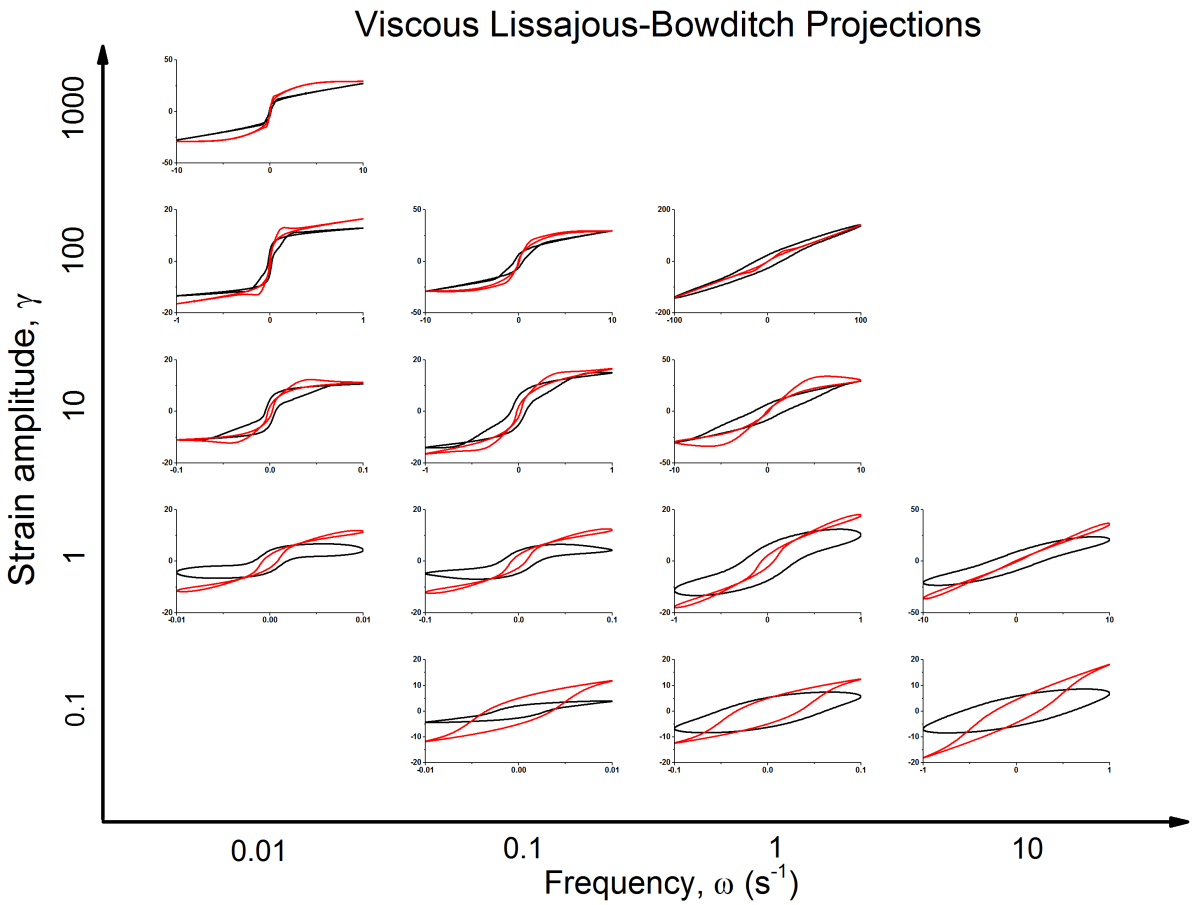

Figure S5: Viscous Lissajous model predictions of LAOS experiments at different strain amplitudes (γ) and frequencies (ω). The x-axis on the inset figures is the strain rate (s^{-1}) and the y-axis is the shear stress (Pa).

5. Predictions of Flow Cessation Experiments

The final test of the model is its application to a flow cessation experiment. In this experiment, the suspension is initially sheared at a given shear rate until it attains a steady state shear stress. Subsequently, the shear rate is rapidly reduced to zero (operationally it is set to $1x10^6$ s^{-1}). The model predictions are compared to the experimentally measured rheology in Fig. **??**. This experiment allows us to examine the relaxation of the elastic strain, γ_e, as the aggregate size does not change over the timescale of this experiment. Therefore, the rheological response observed in this experiment is solely attributable to the changes in the elastic strain stored by the microstructure. The model captures the initial stress transients in the flow cessation experiment with an initial shear rate of 0.25 s^{-1}. However, it increasingly deviates from experimental measurements for flow cessation experiments starting from higher shear rates as shown in the same figure. This discrepancy can be partially attributed to the simple relaxation time used in the model. Still, the key point here is the ability to capture some of the general trends seen in the experimental data.

While the aggregate volume fraction remains unchanged over the experimental timescales, the elastic strain shows dramatic changes and accounts for the transient behavior seen in the model predictions of the shear stress. In addition, although not shown here, the model also predicts an eventually recovery of the shear stress to a final value that equals the yield stress at very long timescales of the order of 10^6 seconds.

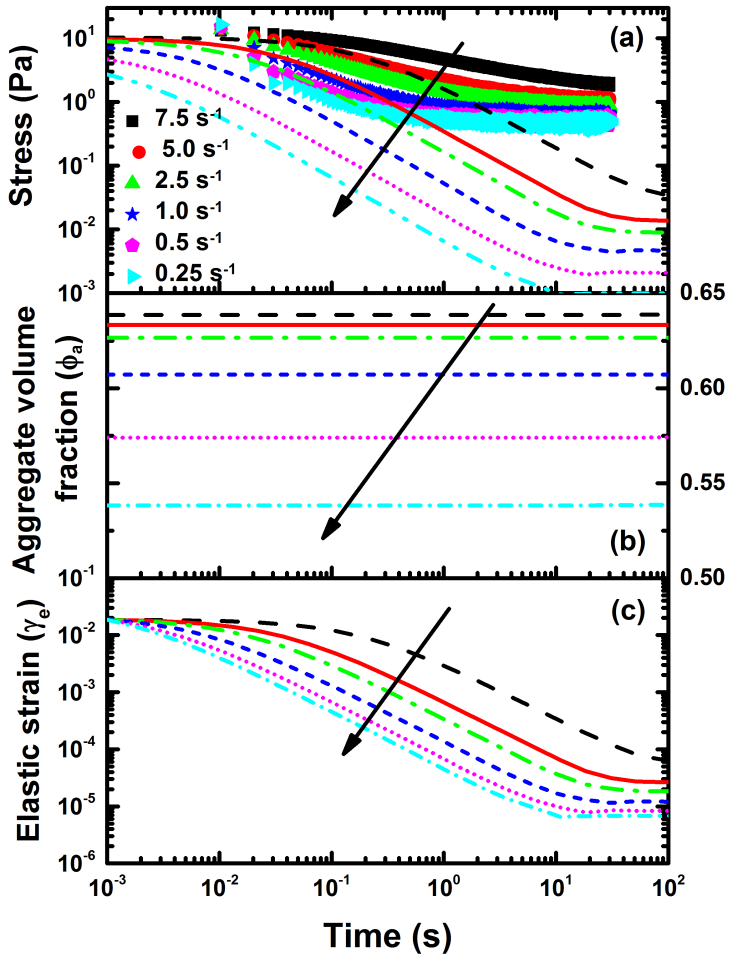

Figure S6: Model predictions showing the shear stress as a function of time for flow cessation experiments. Initial shear rates indicated above and final shear rate in all cases is $1x10^6$ s^{-1}. Arrows indicate decreasing initial shear rate in flow cessation experiments. (a) The evolution in shear stress as a function of time. (b) Structural predictions of the aggregate volume fraction as a function of time. (c) The evolution of the elastic strain as a function of time.

6. Summary of Model Parameters from Simulated Annealing

The best set of parameters reported in the main paper were obtained from 15 iterations of the simulated annealing algorithm developed by Armstrong et al. [**?**]. In Table 1, the best fits corresponding to each of the 15 iterations is summarized as well as the average value and standard deviation of each parameter. In Table 2, a correlation matrix is presented to examine whether any of the parameters are correlated, to explore the possibility of future model reduction. Table 3 presents a qualitative summary of the meaning of the various values of the correlation coefficients appearing in Table 2 adopted from Cohen [**?**].

Table 1: Summary of model parameters over 15 independent runs of the simulation annealing algorithm. Values in boldface indicate parameters resulting in smallest objective function value.

Run number	α	W	b_o	R_h/R_a	d_f	m_p	F_{obj}
1	**0.61**	**4.08**	**0.008**	**0.92**	**2.11**	**468.26**	**0.014**
2	0.89	5.74	0.020	0.91	2.11	658.02	0.0170
3	0.79	51.30	0.014	0.92	2.23	3572.72	0.0207
4	0.49	96.71	0.013	0.90	2.18	2178.22	0.0215
5	0.75	26.24	0.014	0.92	2.23	3895.56	0.0219
6	0.69	91.76	0.009	0.88	2.27	8212.48	0.0223
7	0.40	8.16	0.004	0.88	2.12	449.30	0.0224
8	0.62	46.36	0.005	0.86	2.32	20493.17	0.0224
9	0.74	88.17	0.018	0.84	2.23	5566.20	0.0228
10	0.96	6.00	0.025	0.93	2.16	1128.65	0.0230
11	0.19	96.14	0.007	0.87	2.26	9919.32	0.0237
12	0.94	63.00	0.036	0.86	2.18	2637.63	0.0239
13	0.72	68.49	0.015	0.85	2.30	18142.98	0.0240
14	0.74	64.18	0.016	0.85	2.31	23883.71	0.0247
15	0.89	45.49	0.024	0.95	2.15	1016.65	0.0242

Table 2: Correlation matrix of parameters. The values in boldface indicate Pearson correlation values (r) that are statistically significant with p-values less than 0.05

	α	W	b_o	R_h/R_a	d_f	m_p
α	1.00					
W	-0.32	1.00				
b_o	**0.78**	-0.04	1.00			
R_h/R_a	0.32	**-0.57**	0.15	1.00		
d_f	-0.15	**0.60**	-0.24	**-0.65**	1.00	
m_p	-0.15	0.39	-0.27	**-0.67**	**0.89**	1.00

Table 3: Interpretation of the Pearson correlation values in Table 2.

Pearson Coefficient Value	**Strength of Correlation**
$0.1 < \|r\| < .3$	small correlation
$0.3 < \|r\| < .5$	medium/moderate correlation
$\|r\| > .5$	large/strong correlation

7. Modification to Improve Agreement with Experimental Timescales

In the main paper, in the discussion regarding the comparison of the model predicitons to a step-down experiment from 5 s^{-1} to 0.1 s^{-1} in Fig. 5, we observed that the model predicts much longer timescales that observed experimentally. This was attributed to the evolution of the elastic strain γ_e. This hypothesis is examined by selecting a different relaxation time given by

$$\tau = \frac{\gamma_{lin}}{\dot{\gamma}\left(\phi_a\right)} \left| \frac{\gamma_{lin}}{\gamma_e} \right|^6 , \tag{1}$$

and computing the corresponding model predictions of the step-down experiments. All the parameters in the model are kept at the same level as those reported in the main paper. The implications of the new relaxation time on step-down experiments as well as flow cessation experiments (see Section 5 above) are presented below in Figs. **??** and **??** respectively. In both cases, it is clear that the relaxation term improves quantitative agreement with experimental data. This suggests further improvements in the model will likely rely on modifications to the elastic contributions appearing in the proposed constitutive equation.

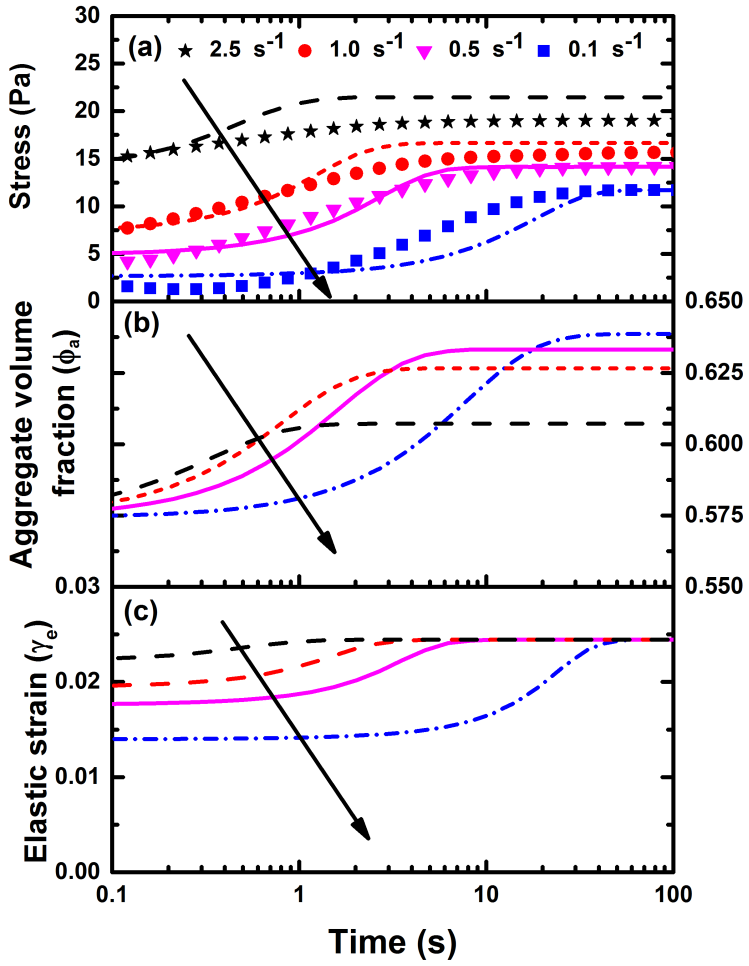

Figure S7: Model fits to step-down experiments using the new relaxation time in Eq. **??**. The initial shear rate is 5 s^{-1} and at time t=0 the shear rate is changed to the final values indicated on the graph. In all cases, arrows indicate direction of decreasing final shear rate. (a) Shear stress as a function of time for step-down transient experiments. (b) Structural predictions of the aggregate volume fraction as a function of time. (c) The evolution of the elastic strain as a function of time.

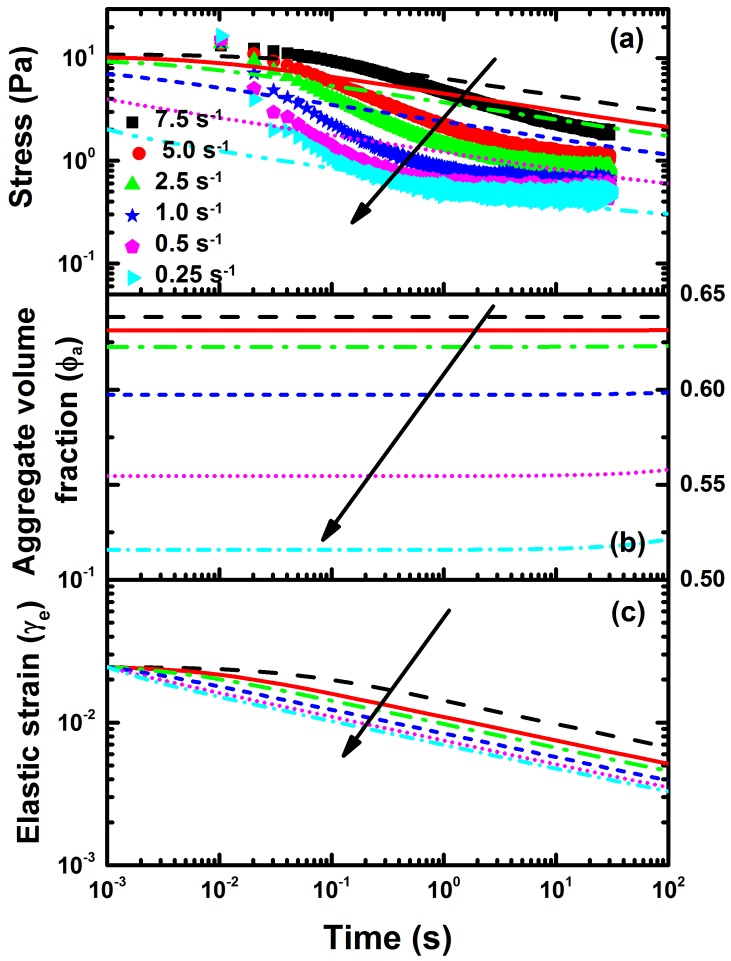

Figure S8: Model predictions showing the shear stress as a function of time for flow cessation experiments using the new relaxation time in Eq. **??**. Initial shear rates indicated above and final shear rate in all cases is $1x10^6$ s^{-1}. Arrows indicate decreasing initial shear rate in flow cessation experiments. (a) The evolution in shear stress as a function of time. (b) Structural predictions of the aggregate volume fraction as a function of time. (c) The evolution of the elastic strain as a function of time.

References

[1] Armstrong MJ, Beris AN, Rogers SA, Wagner NJ. Dynamic shear rheology of a thixotropic suspension: Comparison of an improved structure-based model with large amplitude oscillatory shear experiments. *J Rheol.* 2016;60:433-450.

[2] Cohen J. *Statistical power analysis for the behavioral sciences.* Hilsdale, New Jersey: Erlbaum, 1988.